Effects of Steel Cell Components on Overall Capacity of Pulsed Laser Deposited FeF_2 Thin Film Lithium Ion Batteries

Shadi Al Khateeb,[a,b,z] Aaron G. Lind,[b] Reinaldo Santos-Ortiz,[c] Nigel D. Shepherd,[c] and K. S. Jones[b]

[a]*Department of Materials Engineering, Faculty of Engineering, Al-Balqa' Applied University, Al-Salt 19117, Jordan*
[b]*Department of Materials Science and Engineering, University of Florida, Gainesville, Florida 32611, USA*
[c]*Department of Materials Science and Engineering, University of North Texas, Denton, Texas 76203, USA*

130 nm FeF_2 films were deposited on AISI 304 steel substrates by pulsed laser deposition for use as cathodes in lithium ion batteries (LIBs). Aluminum and steel leads pouch cells as well as coin cell battery configurations were used to determine the effect of cell materials on galvanostatic and cyclic voltammetry tests. It was observed that there is a large increase in measured capacity for FeF_2 films cycled using pouch cells with steel leads relative to pouch cells using aluminum leads. Transmission electron microscope (TEM) imaging showed similar microstructural behavior of the cycled FeF_2 films irrespective of the use of steel leads or aluminum leads. Results of X-ray photoelectron spectroscopy and galvanostatic testing on bare stainless steel substrates suggest that the increase in capacity for cell configurations using steel components is due to the cycling of surface iron oxides and this can be avoided through the use of Al leads.
 [DOI: 10.1149/2.0021509jes]

Manuscript submitted January 6, 2015; revised manuscript received May 26, 2015. Published June 6, 2015.

Pouch cell batteries are widely used to investigate the performance of cathodes, such as $LiFePO_4$,[1] TiO_2,[2] $Li_4Ti_5O_{12}$,[3] $LiNi_{0.8}Co_{0.15}Al_{0.05}O_2$,[4] and anodes[5,6] in lithium ion batteries (LIBs). Different types of current collectors and tab leads were used in the cell assembly such as aluminum, steel, nickel and copper,[1,4,7] but it is not well documented how the cell materials can contribute to the total capacity of these thin film batteries. The goal of this work is to study what effect cell component choice and cell design have on the measured capacity of thin film lithium ion batteries, irrespective of the thin film cathode material type. Lithium metal anodes and the FeF_2 cathode films deposited by pulsed laser deposition (PLD) were used for this work. The attractiveness of PLD-deposited FeF_2 is an attractive material for thin film lithium ion conversion cells due to the high reported theoretical capacity of 571.2 mAh/g[8] which gives it a distinct advantage over conventional cathodes of intercalation compounds such as $LiCoO_2$ and $LiFePO_4$ with capacities of 120–200 mAh/g.[9–11] Compared to other conversion materials, FeF_2 has higher capacity than SnF_2 (342 mAh/g), BiF_3 and comparable capacity to CrF_2,[12] but FeF_2 has the advantage that Fe is more earth abundant than Sn, Bi and Cr which is important for wide scale use of batteries. Previous investigations of FeF_2 as a cathode material in lithium ion cells have resulting in measured capacities ranging from 130 mAh/g to near theoretical capacity with the large range in measured capacities generally being attributed to differences in FeF_2 processing or cycling conditions.[8,13–16] FeF_2 films deposited by PLD reported an increase in capacity upon cycling which was attributed to the oxidation of Fe due to the contamination of oxygen from the electrolyte. The increase in capacity was also postulated to be due to formations of a SEI layer caused by electrolyte decomposition.[8] The FeF_2 nature of these batteries result in batteries with low to high total capacity using coin cell configuration which are steel-made from one hand. From the other hand one of the possible pouch cell components would be the metallic leads which usually have a thin oxide layer on the surface. Reports investigated the application of the Fe_3O_4 oxide films and porous hollow Fe_3O_4 beads[8,17] as a potential cathode material in LIBs. They found that the Fe_3O_4 exhibits a capacity of 500–900 mAh/g, depending on how the iron oxide was made, with a discharge potential of 1–1.5 V and a corresponding charge potential of 1.2–2.2 V. The principal electrochemical process occurring during the charge and discharge cycles of Fe_3O_4 proceeds as[18]

$$Fe_3O_4 + 8e^- + 8Li^+ \leftrightarrow 3Fe^0 + 4Li_2O$$

As Fe_3O_4 is a conversion material then using FeF_2 conversion cathodes in investigating the effect of current collectors on the capacity of LIBs is an advantage, to reduce the variables in this study, compared to conventional cathode materials which are intercalation compounds. Nevertheless studying the effect of steel leads contribution to the capacity of LIBs using conventional cathode materials would be an interesting subject to investigate.

Attempts were also made to improve the gravimetric capacities of anodes through the development of light-weight current collector.[5,19] Aluminum has been long investigated as a potential anode for lithium ion batteries due to its low potential versus Li, high theoretical capacity (~933 mAh/g for LiAl), low cost, and abundance, but did not receive much attention due to it slow performance.[20–22] Aluminum has also been investigated as a possible anode for LIBs in the form of a foil,[23] film deposited on copper support,[22] powder,[24,25] nanowires with naturally oxidized Al_2O_3 surface layer[26] and thin film of aligned aluminum nanorods.[27] Aluminum anodes charge potentials near 0.2 V and discharge potentials near 0.55 V were reported irrespective of the aluminum structure.[22–27] Yet despite all its advantages, aluminum anodes fail due to pulverization, even for a nanowire ≈50 nm in diameter[20,26] and recent studies have not shown stable reversibly cycling using aluminum as an active anode material.[20,22,23] Other investigations reported that aluminum foil was found to be the most suitable material as a current collector for the cathodes in LIBs due to its stability against electrochemical oxidation.[28,29] Another study on 304 stainless steel revealed the formation of a passive layer of (Fe, Cr)-oxide, on which (Cr, Fe)-fluorides reside that would improve the corrosion resistance in the presence of $LiPF_6$ salt[30] and accordingly it was claimed the possibility of using such steel as applicable current collectors for both positive and negative electrodes, and cell cases for LIBs.[30]

Our initial investigation into the capacity of PLD-deposited FeF_2 films resulted in much lower capacities for cells made with aluminum leads compared to stainless steel leads for the same cycling conditions. Although steel and aluminum have been investigated as an anode and cathode, to the authors' knowledge, no reports were found investigating the contribution of steel and/or aluminum leads to the capacity of LIBs. This work studies what effect cell component choice (steel and aluminum leads) and cell design (pouch cell

[z]E-mail: icytecry@yahoo.com

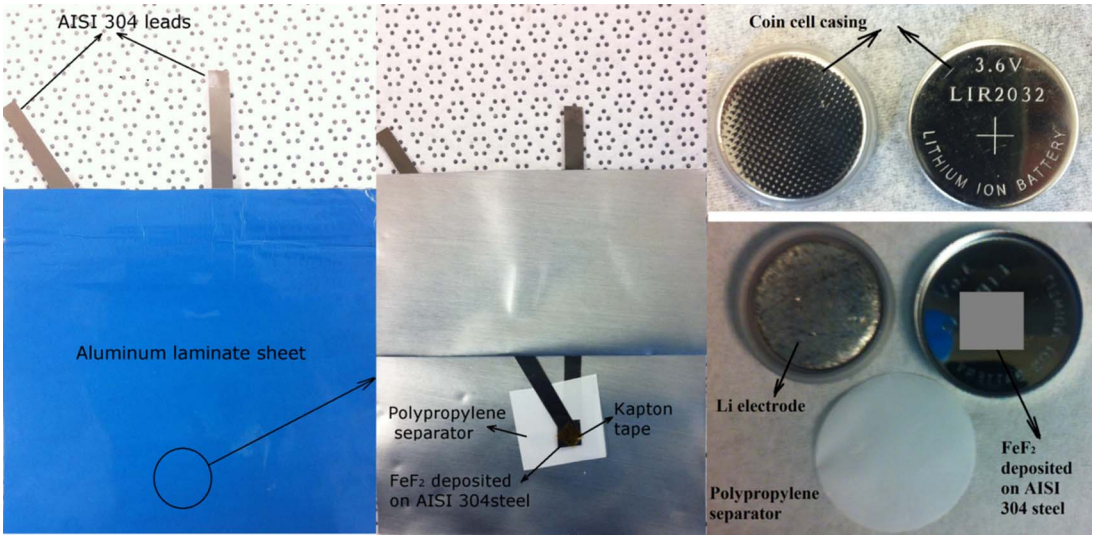

Figure 1. Pouch cell battery (left) and steel coin cell battery (right) showing the different components. The coin cell picture was taken in Ar-filled glove box. The images are not to scale i.e. the the coin cell has a diamter of 2 cm and is just magnified to make it clearer.

configuration compared to coin cell configuration) have on the measured capacity of thin film FeF_2 LIBs in effort to document how the cell materials can contribute to the measured capacity of thin film FeF_2 cathodes using pouch cell batteries. A detailed study investigating the effect of C-rate on the obtained capacities and the corresponding microstructural evolution can be found elsewhere.[31]

Experimental

130 nm FeF_2 films were deposited via PLD of FeF_2 targets (fabricated from anhydrous FeF_2 powder of 99% purity: Alfa Aesar) onto 0.5 cm × 0.5 cm × 25 μm AISI 304 stainless steel substrates (current collectors) (Trinity Brand Industries) held at 400°C at a base pressure of $4–5\times10^{-7}$ torr. Pulses of a 248 nm KrF laser were performed at a frequency of 10 Hz with a fluence of 3.75 J/cm^2 using Lambda Physik, Compex 201. After PLD deposition onto the stainless steel substrate, test cells were assembled inside a glove box in Ar ambient with less than 0.1 ppm H_2O. Fig. 1 shows the construction of the pouch cells with aluminum and AISI 304 stainless steel leads (as well as the 2032 coin cell batteries that were used in this study). 0.75 cm × 0.75 cm × 0.38 mm Lithium metal anodes (99.9% purity, Sigma Aldrich), 1.5 cm × 1.5 cm × 21.5 μm Celgard C480 polypropylene separators, and FERRO electrolyte solutions consisting of 1 M $LiPF_6$ in dimethyl carbonate : ethylene carbonate (DMC:EC) (1:1 by volume) were used for all cell variations studied in this work. The purity of $LiPF_6$ was 99.8% and the water content of the electrolyte was 20 ppm maximum, In the construction of the pouch cells the aluminum laminate sheets were heat sealed together to form the body of the pouch. The first heat seal occurred at the leads which were positioned in a (V) shape. The electrodes were attached to the leads with a piece of Kapton tape. Electrochemical characterization of the assembled cells was performed using galvanostatic and cyclic voltammetry measurements using a Arbin BT2000 over a potential window of 1–4.5 V. Galvanostatic tests were performed at a C-rate of C/1 while cyclic voltammetry was performed at 1 mV/s. Chemical characterization was performed using X-ray photoelectron spectroscopy (XPS: Φ ULVAC-PHI, inc., PHI 5000 VersaProbe II). The XPS spectra were recorded with a standard Mg Kα source using 23 pass energy, 0.1 eV step, and 20 milliseconds per step for the detailed spectra. Cross sectional TEM (X-TEM) samples were prepared using an in situ Focused ion beam (FIB: FEI dual-beam Strata DB 235) technique described elsewhere[32] and structural characterization was carried out with transmission electron microscopy (TEM: JOEL 2010F).

The mass of the deposited FeF_2 films were calculated from X-TEM measurements of film thicknesses, deposition areas (which would be similar to the areas of the of the films' substrates) and the known density of the FeF_2 targets (3.0 g/cm^3). For the 130 nm FeF_2 film deposited on 0.5 cm × 0.5 cm substrate the mass/area is 5.1×10^{-5} g/cm^2.

Results and Discussion

Fig. 2 shows the BF-TEM and selected area electron diffraction (SAED) of the as-deposited 130 nm FeF_2 films. Peaks from the

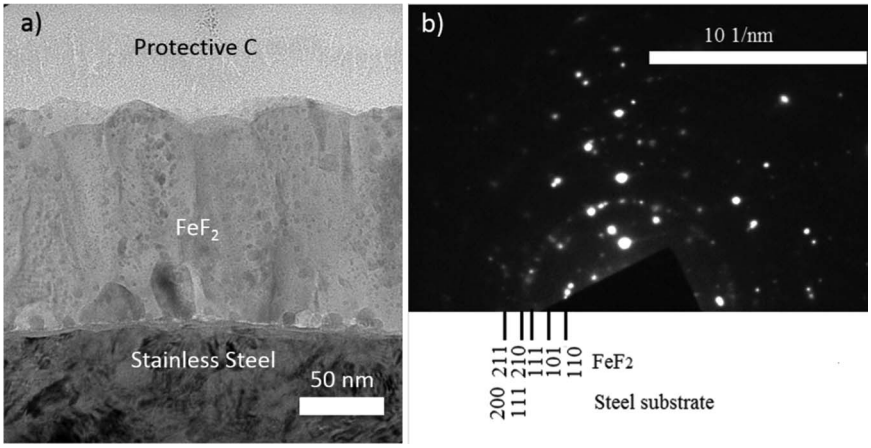

Figure 2. a) Bright field TEM image of as-deposited 130 nm FeF_2 film deposited by PLD and b) the corresponding selected area electron diffraction pattern.

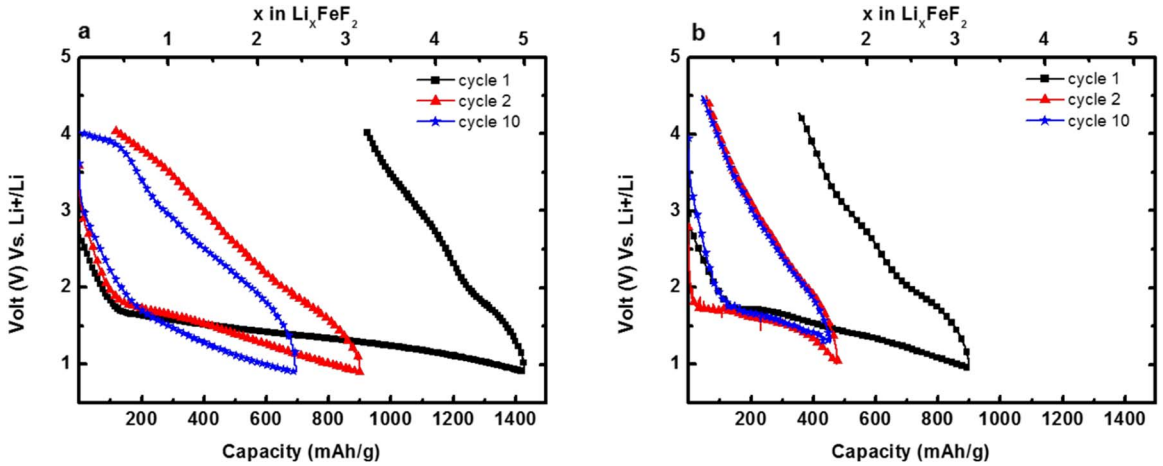

Figure 3. Discharge-charge curves for the 50 nm FeF_2 film cycled in a voltage window of 1–4.5 V at a C-rate of C/43 using pouch cell with a) steel leads and b) aluminum leads. Capacity (mAh/cm^2) = capacity (mAh/g) (6×10^{-5}).

stainless steel current collector and FeF_2 were identified from SAED using the standard JCPDS files 00-033-0397 and 01-071-1968 for stainless steel and FeF_2, respectively, indicating that polycrystalline FeF_2 had been deposited on the stainless steel substrates. FeF_2 films cycled at C/43 using pouch cells with steel and aluminum leads (Fig. 3a and Fig. 3b, respectively) show capacities larger than the theoretical value when using the steel leads pouch cells. Further investigation on the effect of C-rate on the measured capacities of FeF_2 films is discussed elsewhere.[31] For time saving the films will be cycled at faster C-rate (C/1) from now on. Fig. 4 shows the cyclic voltammograms of cells made from 130 nm thick PLD-deposited FeF_2 films using the pouch cell configuration with stainless steel leads, aluminum leads, and 2032 coin cells. It is immediately evident from the results in Fig. 4 that the measured cycling behavior of the FeF_2 films was influenced by cell construction. Previous authors have identified peaks at 3 V during charging and 1.75 V during discharge for FeF_2 cathodes,[8,13,14,33] consistent with what was observed in both the coin cell and aluminum lead pouch cells but in the case of stainless steel lead pouch cells, a distinct peak is observed in the cyclic voltammograms in Fig. 4a at 2 V. The results of the galvanostatic test (capacity vs. cycle number and the corresponding discharge-charge curves) of 130 nm FeF_2 films using stainless steel and aluminum lead pouch cells

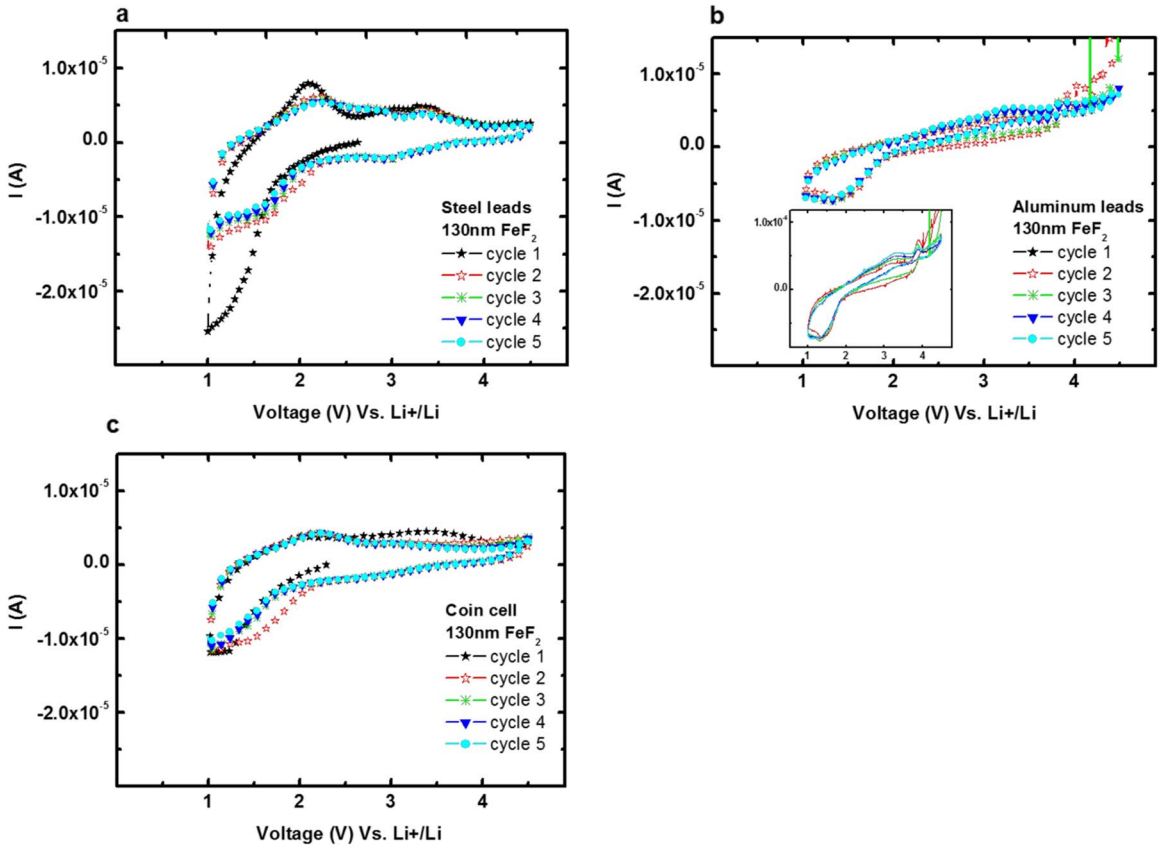

Figure 4. Cyclic voltammogram at a scan rate 1 mV/sec in a potential window of 1–4.5 V for 130 nm FeF_2 deposited by PLD for a) pouch cell with stainless steel leads, b) pouch cell with aluminum leads, and c) coin cell.

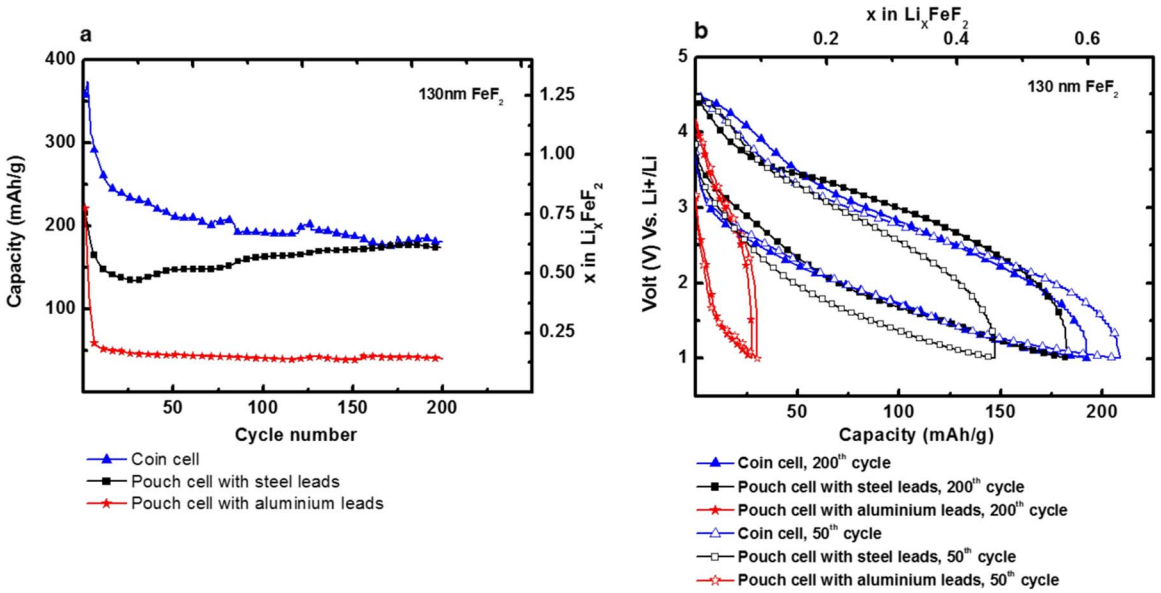

Figure 5. a) Galvanostatic test performed at a C-rate of C/1 for 130 nm FeF_2 deposited by PLD for a pouch cell with stainless steel leads, a pouch cell with aluminum leads, and a coin cell b) Corresponding discharge–charge curves. For pouch cells, capacity (mAh/cm^2) = capacity (mAh/g) (6×10^{-5}). For coin cells, capacity (mAh/cm^2) = capacity (mAh/g) (0.8×10^{-5}).

as well as the coin cell configuration is shown in Fig. 5. Despite all FeF_2 cathodes being of the same size and thickness and thus having the same specific capacity, the measured specific capacity for these films is shown to depend on cell leads and type. A second set of electrochemical tests were performed on cells without any FeF_2 cathodes, i.e. bare steel substrates with an area of 0.25 cm^2 were used, to determine if the measured capacity was a result of the cell components themselves. Fig. 6 shows the cyclic voltammograms of cells without FeF_2 cathodes. Pouch cells made with aluminum leads do not show a peak at 2 V but pouch cells made with stainless steel leads and the coin cells show the peak at 2 V, though it is less pronounced in the coin cell configuration, indicating that the stainless steel leads were

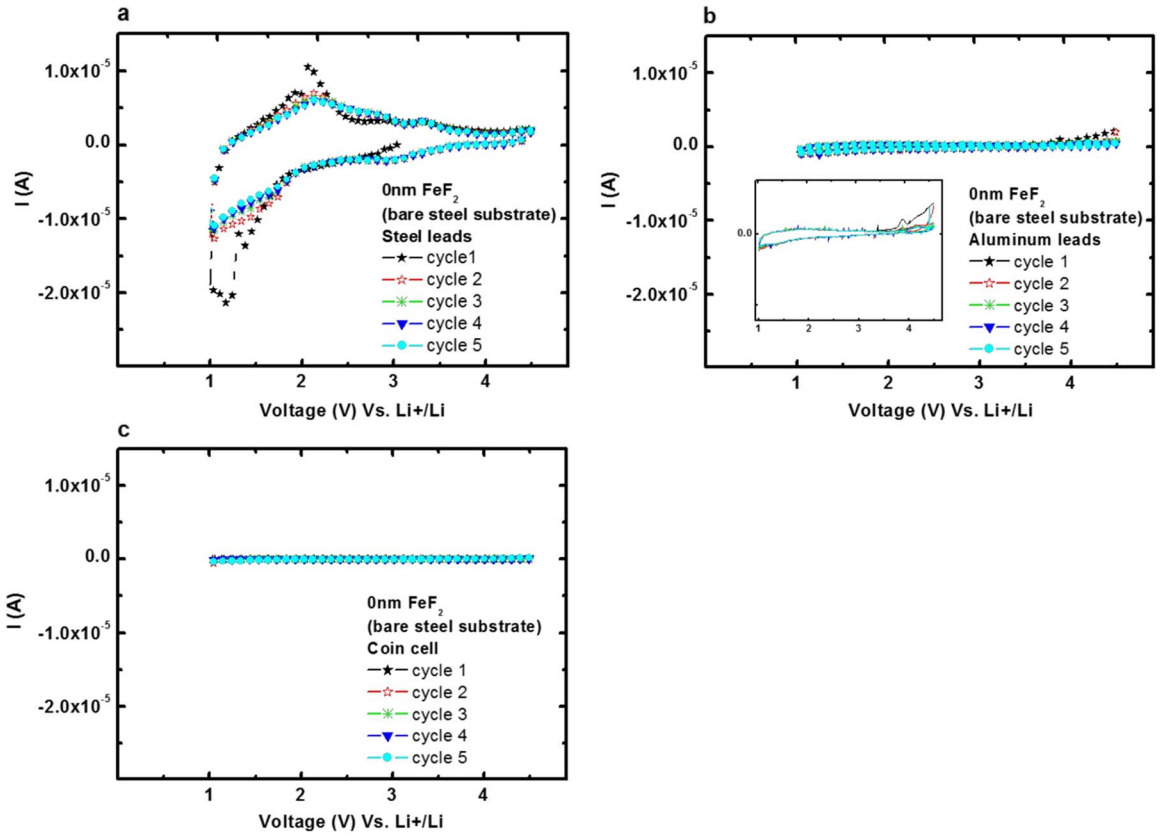

Figure 6. Cyclic voltammogram at a scan rate 1 mV/sec in a potential window of 1–4.5 V of bare steel substrates for a) pouch cell with stainless steel leads (with area of 3.16 cm^2), b) pouch cell with aluminum leads, and c) coin cell.

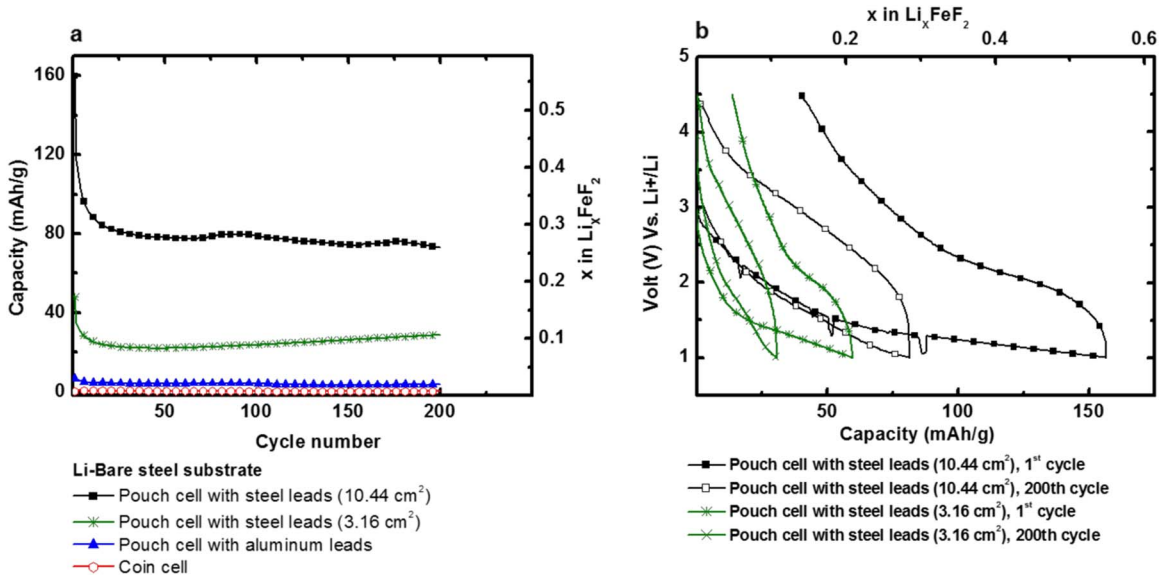

Figure 7. a) Galvanostatic test performed at a C-rate of C/1 of bare steel substrates for a pouch cell with stainless steel leads, a pouch cell with aluminum leads, and a coin cell b) Discharge-charge curves of the bare steel substrates cycled using pouch cells with stainless steel leads. For pouch cell, capacity (mAh/cm^2) = capacity (mAh/g) (6×10^{-5}). For coin cells, capacity (mAh/cm^2) = capacity (mAh/g) (0.8×10^{-5}).

likely contributing the measured capacity. It is worth noting that the coin cell batteries themselves are also made of stainless steel, however for the coin cell construction only the substrate with an area of 0.25 cm^2 would be facing the electrolyte-impregnated separator (by 1 to 2 drops) and no other coin cell components would be in direct contact with the electrolyte as opposed to the pouch cell construction where the total steel lead area is in direct contact with electrolyte (0.75–1 ml). The area of the steel lead in contact with electrolyte inside the pouch cell (Fig. 1) was calculated for the two faces of the lead, ignoring the area along the lead thickness due to its small dimension (25 μm), and by subtracting the area covered with Kapton tape used for the attachment of the electrodes to the leads. The reduction and elimination of the peak at 2 V in coin cells and pouch cells with aluminum leads, respectively can be attributed to the small total surface area of the steel exposed to the electrolyte (0.25 cm^2) compared to the use of the pouch cell with steel leads where the total surface area of the steel substrate and its steel leads exposed to the electrolyte ranged between 3.41–10.69 cm^2. Galvanostatic tests of the bare substrates (capacity vs. cycle number and corresponding discharge-charge curves for FeF_2 films cycled using pouch cells with steel leads) shown in Fig. 7 confirm that the specific capacity was much higher for pouch cells with stainless steel leads (especially with large lead area) compared to the cell with aluminum leads and coin cell configurations. The capacity values in Fig. 7 are not absolute as a 130 nm FeF_2 thickness on the bare current collectors was assumed in capacity calculations for the sake of comparison. Higher measured capacity of the coin cell with 130 nm of FeF_2 relative to the stainless steel lead pouch cells (Fig. 5) was detected. Correcting capacities to mAh/cm^2 show lower capacity of the FeF_2 films cycled using coin cell configuration compared to the one obtained when cycling FeF_2 films using pouch cell with steel leads. The lower capacity of the FeF_2 films cycled with coin cell configuration may be attributed to the smaller area of the steel components exposed to the electrolyte. The cyclic voltammograms for pouch cells with aluminum leads (insets in Fig. 4b and Fig. 6b) show charge peaks at 3.9 V which have also been observed by others[16] using coin cells in their investigation but the cause of these peaks are still under investigation.

The low charge and discharge potentials of aluminum anodes (0.2 V and 0.55 V, respectively)[22–27] compared to FeF_2 cathodes (3 V and 1.75 V, respectively)[8,13,14,33] and Fe_3O_4 cathodes (1.2–2.2 V and 1–1.5 V, respectively)[8,17] make aluminum leads more attractive for use in lithium ion pouch cell batteries with FeF_2 as it will not contribute to the capacity of FeF_2 films in the potential range applied in this work (1–4.5 V) as seen in Fig. 6b and Fig. 7 compared to Fig. 4 and Fig. 5, respectively.

Fig. 8 shows the post cycling morphology of FeF_2 films for both the stainless steel and aluminum lead pouch cells. Both the aluminum lead and steel lead pouch cells show similar cycling of the FeF_2 which further indicating that the differences in capacity were un-related to the FeF_2 films themselves and that the likely reason for the high measured capacity in the stainless steel pouch cells. Comparison of post-cycling films in Fig. 8 with the as-deposited film in Fig. 2a indicates that an expansion of 11% along the film's thickness occurred during cycling at C/1. The corresponding capacity obtained from cycling FeF_2 using a pouch cell with aluminum leads is 55 mAh/g as shown in Fig. 5. Incomplete conversion of FeF_2 in this case is not unexpected given the relatively high C-rate of C/1 used in this work. The microstructural evolution and its relation with obtained capacity of the FeF_2 films after cycling is discussed further elsewhere.[31]

The increase in capacity of FeF_2 by the oxidation of Fe due to the contamination of oxygen from the electrolyte or by the formation of a SEI layer caused by electrolyte decomposition[8] is inconsistent

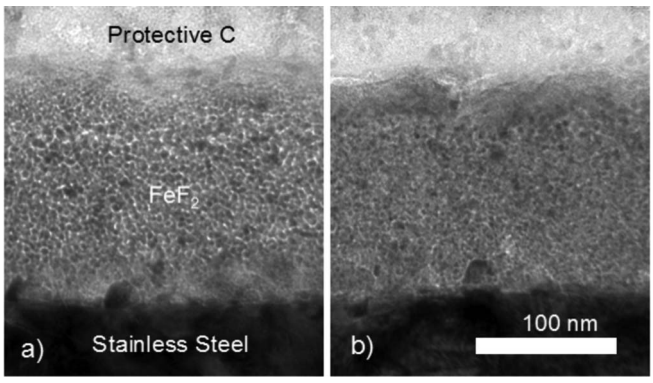

Figure 8. Bright field TEM images of the 130 nm FeF_2 film after galvanostatic cycling for 200 cycles at a C-rate of C/1 using pouch cells with a) aluminum leads b) steel leads. The FeF_2 film is coated with a protective carbon (C) to protect the sample surface from amorphization due the ion beam during X-TEM sample preparation.

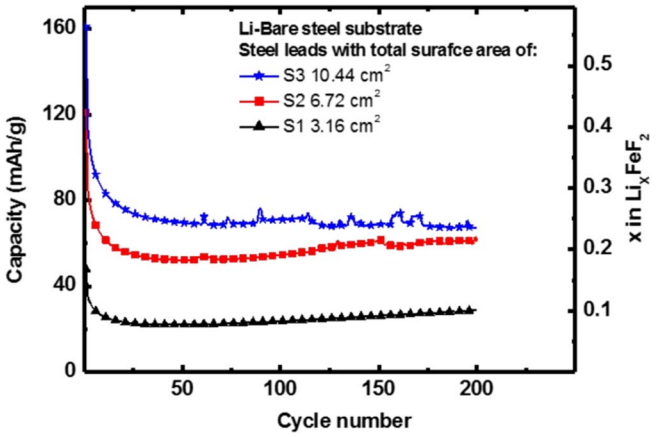

Figure 9. Galvanostatic test performed at a C-rate of C/1 of bare steel substrates for a pouch cell with stainless steel leads with total lead areas of 3.16–10.44 cm^2. Capacity (mAh/cm^2) = capacity (mAh/g) (6×10^{-5}).

with the results of this work as the oxygen content in the electrolyte is constant and should not result in an increase in the capacity with increasing the size of the steel leads whereas the SEI formation occurs only in the first cycle which cannot explain the persistent, high capacity observed in this work. However Fe_3O_4 films and porous hollow beads were investigated as a potential cathode material in LIBs.[8,17] Thus it is possible that the surface oxide on stainless steel leads is contributing to the measured capacity. Also it was found that 304 steel passivates in the presence of $LiPF_6$ salt[30] and accordingly may thicken the oxide layer during the cycling which then would contribute the total measured capacity of FeF_2 films. In order to further determine the role of surface oxides from the leads to the total capacity, stainless steel leads of varying sizes were studied in a pouch cell configuration. Fig. 9 shows the galvanostatic test for samples of varying lead sizes. The results show clearly that the measured capacity increases with increasing the total stainless steel lead area (capacity values are not absolute as mentioned earlier).

XPS was used to investigate the oxide on as-received stainless steel substrate as well as stainless steel substrate that had undergone discharge galvanostatic cycling. The presence of an oxide layer was observed for the as received steel substrate, from the Fe $2P_3$ and O 1S peaks. It was determined that there are oxides on the surface and the oxide could potentially be either Fe_2O_3 or Fe_3O_4 or a mixture of the two phases as shown in Fig. 10a and Fig. 10b. A more detailed study of the surface oxide of stainless steel substrates has shown that the top layer of the oxide consists of Fe_3O_4.[34] To confirm whether the oxide layer on the surface of the steel leads was cycling simultaneously with FeF_2, the surface of the as received steel substrate and a cycled steel substrate were sputtered with argon during the XPS measurements. XPS of the as-received steel substrate in Fig. 10a and Fig. 10b indicates that the peaks corresponding to the oxide layer were diminished with the in situ argon sputtering. This was also observed for a galvanostatically discharged steel substrate, however, two peaks for O 1S (Fig. 10c) were detected compared to the as-received substrate. The first peak correspond to the presence of Li_2O at 531.3 eV and the other one appeared during the sputtering process at 530 eV. This indicates the cycling of the oxide layer on the surface of the steel substrate by the formation of a top layer of Li_2O, however the conversion reaction is not complete and this is concluded from the presence of a bottom oxide layer. The incomplete conversion may be consistent with the

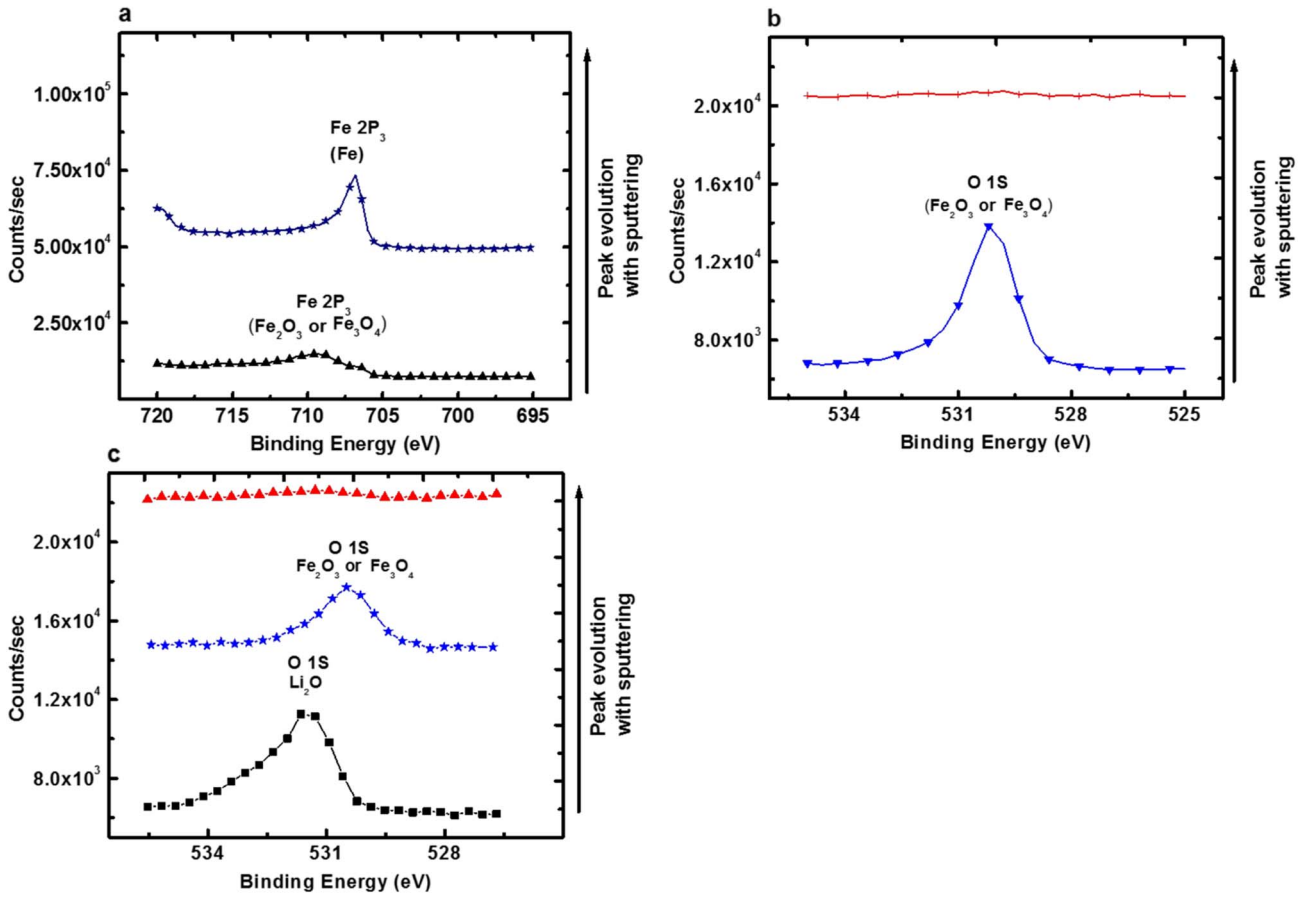

Figure 10. XPS spectra showing the diminishing of the oxide peaks of a) Fe $2P_3$ and b) O 1S with argon sputtering for the as-recieved steel substrate and of c) O 1S for the galvanostatically discharged steel substrates.

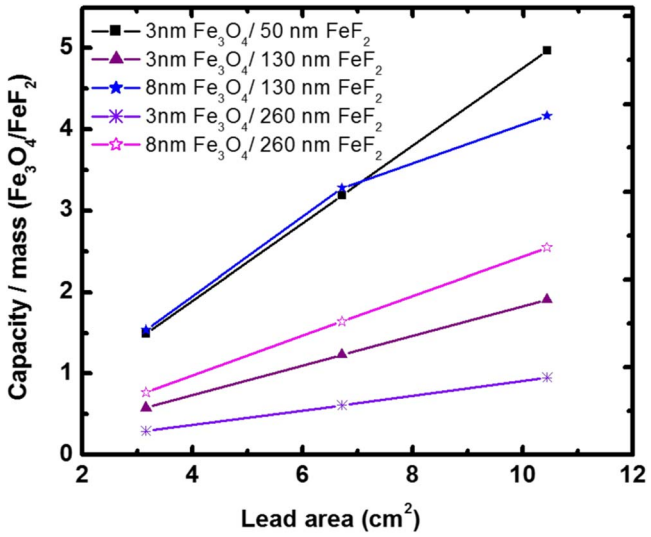

Figure 11. Calculated capacities/mass of Fe_3O_4 relative to FeF_2 as a function of steel lead area. The effect of the FeF_2 films thicknesses, which were deposited on 0.25 cm^2 steel substrate, and the oxide layer thicknesses are shown.

low capacities obtained in Figure 9, which would also be attributed to the fast C-rate applied during the battery cycling. The XPS measurements are insufficient to measure the actual oxide thickness of the as–received and galvansotatically cycled stainless steel leads and future investigation is required for the thickness measurements. An attempt to estimate the iron oxide layer thickness of the leads that would result in the measured cycling currents used in Fig. 9 was made using theoretical values for the specific capacity of 926 mAh/g[17] for Fe_3O_4 and measured values of total stainless steel surface area exposed to the electrolyte and density. The calculated oxide thickness was found to be 3–8 nm and the corresponding oxide capacities at the same cycling current would be 62% more compared to those obtained in Fig. 9.

Based on the above oxide thicknesses and the steel lead areas used in this work (Fig. 9), the theoretical capacities/mass were calculated for Fe_3O_4. Meanwhile the theoretical capacities/mass of FeF_2 films deposited on 0.25 cm^2 steel substrates were calculated for different film thicknesses. Fig. 11 shows the calculated capacity of Fe_3O_4 relative to FeF_2 films based on the mass of the films as a function of the steel leads areas and as affected by the thickness of the oxide layer and FeF_2 films. It is very obvious that the cell performance is dominated by the oxide layer when the capacity ratio is larger than one as evidenced by the 8 nm Fe_3O_4/130 nm FeF_2 and the 8 nm (not shown) and 3 nm Fe_3O_4/50 nm FeF_2 combinations irrespective of the lead area. This result agrees with the large capacity obtained for the 130 nm FeF_2 film in Fig. 5 assuming an oxide thickness of 8 nm. Stainless steel lead areas smaller than 6.72 cm^2 and oxide thicknesses smaller than 8 nm are required to reduce the effect of the oxide layer on the total performance of cathodes with areas of 0.25 cm^2. Thickness of the oxide layer on the surface of the steel will be intrinsic to the lead material leaving the area of the stainless steel leads or the FeF_2 films thicknesses as the controllable variables. Increasing the thickness of the FeF_2 films to 260 nm (see Fig. 10) ensures the dominance of the FeF_2 film on the battery performance over the oxide layer assuming that the whole thickness of FeF_2 will cycle, which is still under investigation. For the pouch cells with aluminum leads the capacity/mass of Fe_3O_4 relative to FeF_2 would be zero as there is no steel in contact with the electrolyte to cycle. Even for the coin cell configuration the electrolyte is present as an impregnation for the separator, which reduces the chances of being in contact with steel component of the cell. However, even if there were a contact then by subtracting the area of FeF_2 substrate of 0.25 cm^2 from the area of the cell casing then the area that is supposed to be in contact with the electrolyte would be 2.89 cm^2 for a 2 cm cell diameter (type 2032). This would give a capacity ratio of 0.52 for the 3 nm Fe_3O_4 / 130 nm FeF_2 and 1.41 for the 8 nm Fe_3O_4 / 130 nm FeF_2 combinations. Based on the capacity of the 130 nm FeF_2 film using the coin cell configuration in Fig. 5 then the performance of the cell is dominated by oxide the assuming an oxide layer thickness of 8 nm and this may explain the large obtained capacity but still this should be further investigated. In other words the performance of the FeF_2 battery is dominated by the FeF_2 film over the oxide layer provided that the ratio of the leads' oxide capacity to FeF_2 capacity is much smaller than one.

Conclusions

In conclusion, it has been demonstrated that test cell configuration and material selection plays an important role in accurately measuring the capacity of thin film batteries. The cyclic voltammetry tests on the films using pouch cells with steel leads or coin cells revealed a peak at about 2 V which were attributed to the cycling of the oxide on the steel components of the cells based on comparison of electrochemical results of bare steel substrates with FeF_2 coated substrates as well as the chemical composition results obtained by XPS and structural characterization using TEM. Pouch cells with aluminum leads eliminated erroneous contributions to capacity observed in cells with stainless steel components such that the resultant measured capacity is due entirely to the PLD-deposited FeF_2 film.

Acknowledgments

The corresponding author acknowledges the Scientific Research Support Fund (SRSF)-Jordan for supporting this work performed at the University of Florida.

References

1. J. Shim and K. A. Striebel, *J. Power Sources*, **119–121**, 955 (2003).
2. M. Pfanzelt, P. Kubiak, M. Fleischhammer, and M. Wohlfahrt-Mehrens, *J. Power Sources*, **196**, 6815 (2011).
3. K. Amine, I. Belharouak, Z. Chen, T. Tran, H. Yumoto, N. Ota, S.-T. Myung, and Y.-K. Sun, *Adv. Mater.*, **22**, 3052 (2010).
4. J. Shim, R. Kostecki, T. Richardson, X. Song, and K. A. Striebel, *J. Power Sources*, **112**, 222 (2002).
5. J. W. Choi, L. Hu, L. Cui, J. R. McDonough, and Y. Cui, *J. Power Sources*, **195**, 8311 (2010).
6. L.-F. Cui, Y. Yang, C.-M. Hsu, and Y. Cui, *Nano Lett.*, **9**, 3370 (2009).
7. S. Slane, A. J. DeAnni, and M. T. Brundage, in *Battery Conference on Applications and Advances, 1999. The Fourteenth Annual*, p. 35 (1999).
8. Y. Makimura, A. Rougier, and J.-M. Tarascon, *Appl. Surf. Sci.*, **252**, 4587 (2006).
9. B. L. Ellis, K. T. Lee, and L. F. Nazar, *Chem. Mater.*, **22**, 691 (2010).
10. M. Sina, K. W. Nam, D. Su, N. Pereira, X. Q. Yang, G. G. Amatucci, and F. Cosandey, *J. Mater. Chem A*, **1**, 11629 (2013).
11. J. B. Goodenough and Y. Kim, *Chem. Mater.*, **22**, 587 (2009).
12. M. F. Parkinson, Architectural Influence of FeF_2 Films on Electrochemical Failure Modes in *Materials Science and Engineering.* The State University of New Jersey (2013).
13. F. Wang, R. Robert, N. A. Chernova, N. Pereira, F. Omenya, F. Badway, X. Hua, M. Ruotolo, R. Zhang, L. Wu, V. Volkov, D. Su, B. Key, M. S. Whittingham, C. P. Grey, G. G. Amatucci, Y. Zhu, and J. Graetz, *J. Am. Chem. Soc.*, **133**, 18828 (2011).
14. M. A. Reddy, B. Breitung, V. S. K. Chakravadhanula, C. Wall, M. Engel, C. Kübel, A. K. Powell, H. Hahn, and M. Fichtner, *Adv. Energy Mater.*, **3**, 308 (2013).
15. Y. Makimura, A. Rougier, L. Laffont, M. Womes, J. C. Jumas, J. B. Leriche, and J. M. Tarascon, *Electrochem. Commun.*, **8**, 1769 (2006).
16. Y. Bai, L.-w. Yang, F. Wu, C. Wu, S. Chen, L.-y. Bao, and W.-l. Hu, *J. Renew. Sustainable Energy*, **5**, 021402 1 (2013).
17. Y. Chen, H. Xia, L. Lu, and J. Xue, *J. Mater. Chem.*, **22**, 5006 (2012).
18. T. Muraliganth, A. Vadivel Murugan, and A. Manthiram, *Chem. Commun.*, 7360 (2009).
19. V. I. Chani, Q. Yang, D. S. Wilkinson, and G. C. Weatherly, *J. Power Sources*, **142**, 370 (2005).
20. N. Nitta and G. Yushin, *Particle & Particle Systems Characterization*, **31**, 317 (2014).
21. M. J. Lindsay, G. X. Wang, and H. K. Liu, *J. Power Sources*, **119–121**, 84 (2003).
22. Y. Hamon, T. Brousse, F. Jousse, P. Topart, P. Buvat, and D. M. Schleich, *J. Power Sources*, **97–98**, 185 (2001).

23. S. P. Kuksenko, *Russ. J. Electrochem.*, **49**, 67 (2013).
24. Zhongxue Chen, Jiangfeng Qian, Xinping Ai, Yuliang Cao, and Hanxi Yang, *Electrochim. Acta*, **54**, 4118 (2009).
25. Xuefeng Lei, Chiwei Wang, Zonghui Yi, Yongguang Liang, and Jutang Sun, *J. Alloys Compd.*, **429**, 311.
26. Y. Liu, N. S. Hudak, D. L. Huber, S. J. Limmer, J. P. Sullivan, and J. Y. Huang, *Nano Lett.*, **11**, 4188 (2011).
27. M. Au, S. McWhorter, H. Ajo, T. Adams, Y. Zhao, and J. Gibbs, *J. Power Sources*, **195**, 3333 (2010).
28. C. Iwakura, Y. Fukumoto, H. Inoue, S. Ohashi, S. Kobayashi, H. Tada, and M. Abe, *J. Power Sources*, **68**, 301 (1997).
29. K. Kanamura, T. Umegaki, S. Shiraishi, M. Ohashi, and Z.-i. Takehara, *J. Electrochem. Soc.*, **149**, A185 (2002).
30. S.-T. Myung, Y. Sasaki, T. Saito, Y.-K. Sun, and H. Yashiro, *Electrochim. Acta*, **54**, 5804 (2009).
31. Shadi Al Khateeb, A. Lind, R. Santos-Ortiz, N. Shepherd, and K. S. Jones, *J Mater Sci*, **50**, 5174 (2015).
32. L. A. Giannuzzia and F. A. Stevieb, *Micron*, **30**, 197 (1999).
33. M. J. Armstrong, A. Panneerselvam, C. O'Regan, M. A. Morris, and J. D. Holmes, *J. Mater. Chem A*, **1**, 10667 (2013).
34. J. C. Langevoort, I. Sutherland, L. J. Hanekamp, and P. J. Gellings, *Appl. Surf. Sci.*, **28**, 167 (1987).